Boundary-Layer Meteorology (2005) 117: 111–129
DOI 10.1007/s10546-004-3407-y

AIRCRAFT OBSERVATIONS OF AIR-MASS MODIFICATION OVER THE SEA OF OKHOTSK DURING SEA-ICE GROWTH

JUN INOUE*, MASAYUKI KAWASHIMA[1], YASUSHI FUJIYOSHI[1] and MASAAKI WAKATSUCHI[1,2]

School of Earth and Atmospheric Sciences, Georgia Institute of Technology, 311 Ferst Dr., Atlanta, GA 30332-0340, U.S.A.; [1]*Institute of Low Temperature Science, Hokkaido University, Sapporo, Japan;* [2]*Core Research for Evolutional Science and Technology (CREST), Japan Science and Technology Agency, Tokyo, Japan*

(Received in final form 14 June 2004)

Abstract. In order to quantitatively investigate the role of leads and sea-ice in air-mass modification, aircraft observations were conducted over the partially ice-covered Sea of Okhotsk. We investigated two cold-air outbreak events with different sea-ice concentrations. In both cases, the difference between the temperatures of surface air and the sea surface (ΔT) dropped rapidly with the accumulated fetch-width of leads up to about 35−40 km, and then decreased very slowly. The surface sensible heat flux originating from open water was about 300 W m^{-2} within a few kilometres from the coast and decreased with increasing accumulated fetch-width. The sensible heat flux was about 100 W m^{-2} on average. These results indicate that the downwind air-mass modification depends mainly on the total (accumulated) extent of open water. The total buoyancy flux ($\overline{w'T_v'}$) calculated by the joint frequency distribution method correlated very well with ice concentration. Such a relationship was not clear in the case of the moisture flux ($\overline{w'q'}$). The ratio between rising thermals ($\overline{w^+T_v^+}$) and cold downdrafts ($\overline{w^-T_v^-}$) differed significantly between upwind and downwind regions; that is, the buoyancy flux was dominated by $\overline{w^+T_v^+}$ in the developing stage of the boundary layer, while $\overline{w^-T_v^-}$ also became important after the development of the boundary layer.

Keywords: Accumulated fetch-width of leads, Leads, Sea-ice Sea of Okhotsk, Turbulent heat flux.

1. Introduction

When a cold air mass breaks out from Siberia in winter, the air-mass modification occurs over a relatively warm sea surface (e.g., the Sea of Okhotsk and the Sea of Japan). As shown in Figure 1, cloud streets sometimes form over the ice-covered area of the Sea of Okhotsk, which implies that a considerable amount of heat and moisture is supplied to the atmosphere from leads and polynyas, even in the mainly ice-covered area.

* E-mail: jun.inoue@eas.gatech.edu

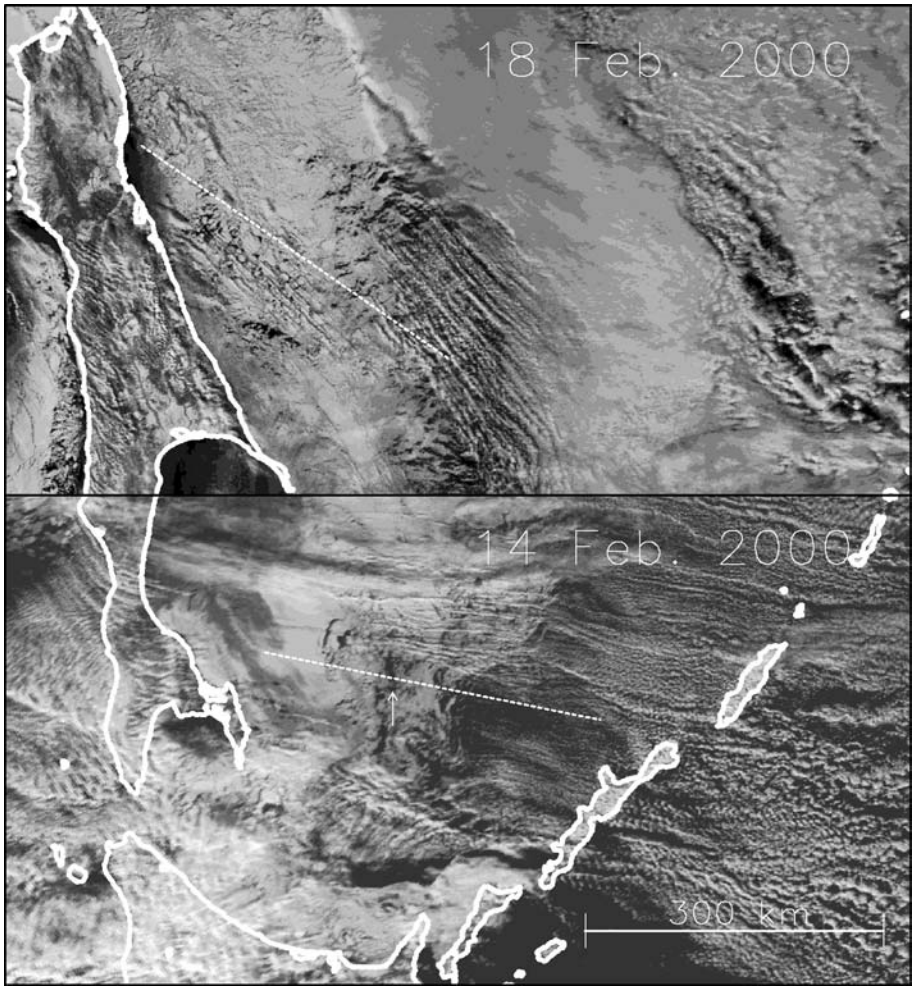

Figure 1. NOAA-14 advanced very high resolution radiometer (AVHRR) imageries of Channel 2 on 0535 UTC 18 February 2000 (upper panel) and on 0442 UTC 14 February, 2000 (lower panel). The dotted line denotes the location of three level flights by the IL-18. An arrow in the lower panel indicates the largest lead along the flight course.

In the Arctic region, the extent of open water (i.e., leads and polynyas) is one of the important factors for the surface heat budget, because the heat exchange through a lead or polynya is two orders of magnitude greater than that through the surrounding snow-covered pack ice (Smith et al., 1990). The presence of even a small percentage of open water in the Arctic Ocean can affect heat budgets in the Arctic region (Maykut, 1978; Ledley, 1988). Further, the fraction of leads is believed to influence the surface energy balance of sea-ice areas through the ice-albedo feedback process (Curry et al., 1995).

The extent of sea-ice in the seasonal-ice zone shows significant interannual variability (e.g., Cavalieri and Parkinson, 1987). The Sea of Okhotsk is the southernmost seasonal-ice zone in the Northern Hemisphere. Some numerical studies pointed out that the sea-ice in the seasonal-ice region possibly influences the atmospheric circulation through dynamic and thermodynamic processes operating both locally and globally (e.g., Okubo and Mannoji, 1994; Honda et al., 1999). However, as they mentioned, sea-ice was treated crudely and heat flux anomalies were exaggerated both in magnitude and scale. It is highly desirable to estimate quantitatively the heat flux over the ice-covered Sea of Okhotsk since this should lead to a better understanding of the role of sea-ice on the local and global atmospheric circulation.

Recently, the surface heat budget and turbulent heat fluxes in the south-western region of the Sea of Okhotsk have been estimated using meteorological data and in-situ ice thickness data observed from an icebreaker, and/or radiosonde data (e.g., Toyota et al., 2000; Inoue et al., 2001; Iwamoto et al., 2001; Ohshima et al., 2003). By treating the turbulent heat fluxes over the open water and sea-ice separately, Inoue et al. (2003) pointed out that the ice concentration is a more important parameter for the estimation of turbulent heat flux than any other meteorological parameter under cold-air outbreak situations. However, the ice concentration was treated coarsely and the spatial variation of air–ice–sea interactions was not examined in their study. Therefore, aircraft observations over the Sea of Okhotsk, similar to those made over the Labrador Sea (Smith and Macpherson, 1996; Renfrew and Moore, 1999), and the Greenland Sea (Brümmer et al., 1992) were desirable to understand the mesoscale and microscale features of the air–ice–sea interaction.

On 14 and 18 February, 2000, we carried out aircraft observations over the south-western part of the Sea of Okhotsk. The objective of this study is to reveal the air-mass modification processes over the Sea of Okhotsk, paying attention to the fraction of leads and polynyas.

2. Aircraft Observations

During a cold-air outbreak we conducted aircraft observations on 14 and 18 February, 2000, using a Russian research aircraft ILYUSHIN-18 (Figure 1). Figure 2 shows the surface weather map at 0000 UTC on 14 and 18 February, 2000. In both cases, the centre of the deepening low was located to the east of the Kamchatka Peninsula. The low pressure in this area and the high pressure over the Siberian continent led to a cold north-westerly wind over Sakhalin Island and the Sea of Okhotsk. The low temperature area, colder than $-12\,^{\circ}C$, over the western part of the Sea of Okhotsk coincides with the area covered by sea-ice, which reduces the heat flux from the ocean to the

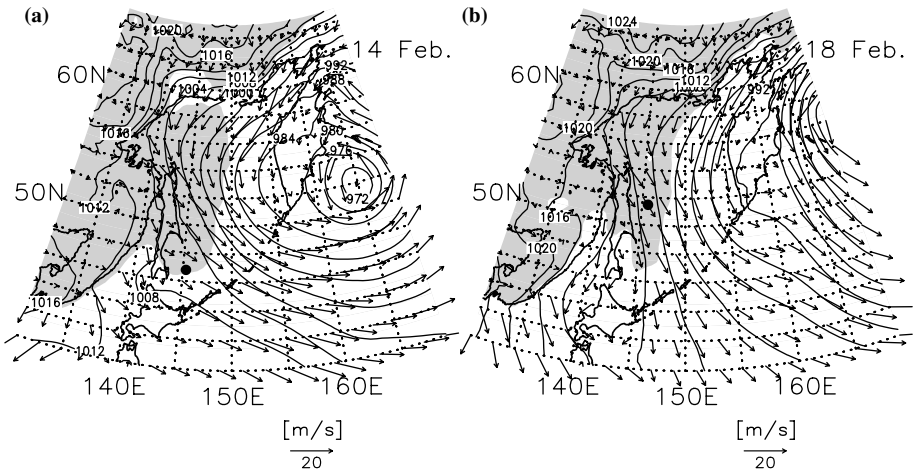

Figure 2. Sea level pressure (hPa) and wind vector (m s^{-1}) on 14 and 18 February, 2000, at 0000 UTC from the ECMWF analyses. The shaded areas indicate air temperatures lower than −12 °C. Observational area on each day is depicted by a closed circle.

atmosphere. As shown in Figure 1, the longitudinal mode of cloud streets developed in the open water downwind, which is evidence of air-mass modification over the sea.

Three measuring level flights (200, 350 and 900 m above the sea surface) parallel to the wind direction at 850 hPa were made on each day. The horizontal length of each level flight was about 300 and 350 km on 14 and 18 February, respectively (dotted line in Figure 1). At the start and end points of the level flights, vertical soundings of the air and dew-point temperatures and wind components were made. The aircraft was equipped with instruments to measure wind speed, wind direction, air temperature, relative humidity, dew point temperature, absolute humidity, and pressure with a 1-Hz-sampling frequency. The aircraft was also equipped with gust probes to measure turbulence quantities, which will be described in Section 5. A visible camera and an infrared camera were installed to continuously record characteristics of the underlying surface conditions (floe size, sea/ice surface temperature, type and amount of cloud, and so on).

3. Sea-ice Conditions

Whether the sea surface is covered with ice or not is very important information for understanding the heat exchange between the sea surface and the atmosphere. In this section, we present the characteristics of ice concentration and surface temperature obtained by visible and infrared cameras.

3.1. Sea-ice concentration

Sea-ice was monitored by a downward-looking visible video camera mounted on the bottom of the aircraft. Images were taken every 130 s. We captured the images every second and gathered digital data with 720 × 480 pixels. The frame area corresponds to 120 m × 80 m when the flight level was 200 m above the sea level. The total frame numbers amounted to 2800 and 3700 on 14 and 18 February, respectively. Figure 3 shows examples of a time series of sea-ice images with different ice concentrations on 14 February. We can clearly observe different sea-ice conditions near the coast of Sakhalin (Figure 3a), a marginal ice zone (Figure 3b), and open ocean (Figure 3c).

Since sea-ice is a strong insulator, it is necessary to calculate the ice concentration precisely. The procedure to calculate the ice concentration is as follows: (1) quantify the brightness of images into 256 grey levels, (2) decide the threshold level between open water and sea-ice, and (3) calculate the number of pixels that exceed the threshold level. Since the threshold level was not constant because of the sun glint, clouds, and the shadows formed by sea-ice and clouds, we determined the threshold level manually from the image, and calculated the ice concentration for each image.

Figure 4a shows the change of ice concentration with distance from the eastern coast of Sakhalin. Within 60 km from the coast, the ice concentration was almost 100%. As shown in Figure 3a, white young ice is predominant in this region and the ice surface seems to be fairly flat. The floe size was estimated to be more than 500 m. On the other hand, the mean ice concentration and mean floe size were reduced to approximately 70% and 50 m (Figure 3b) in the area between 60 and 170 km from the coast. There were some leads of a few kilometres in horizontal scale in this area. The largest lead (10 km) was located at about 130 km offshore from the eastern coast of Sakhalin, which can be clearly recognized from the satellite imagery and is

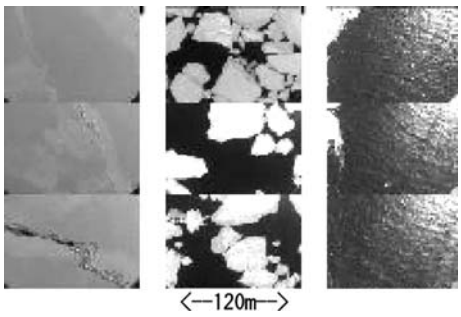

Figure 3. Time series of sea-ice images taken over 3 s at the lowest flight (200 m height) which were taken by the IL-18 in the region of (a) high ice concentration, (b) moderate ice concentration, and (c) low ice concentration, respectively.

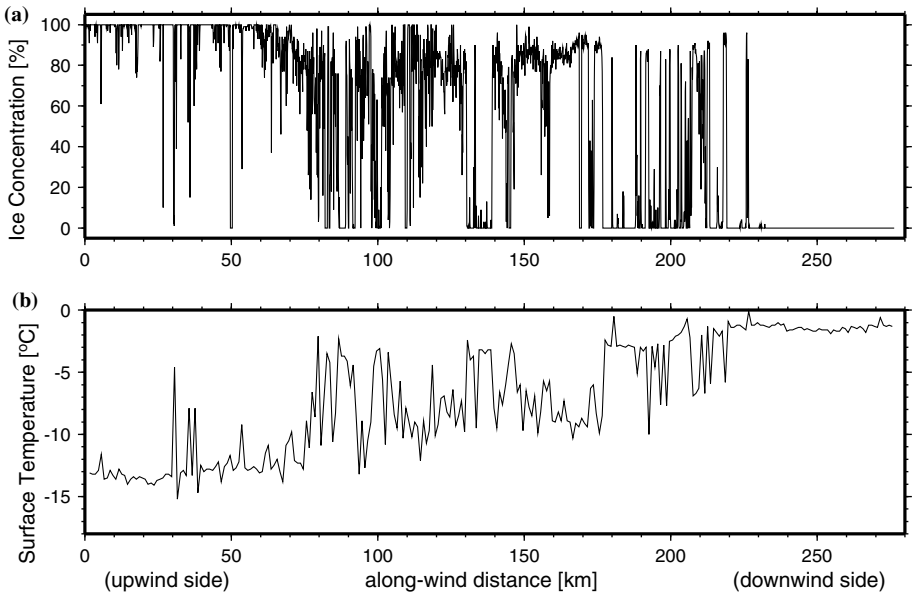

Figure 4. Horizontal distributions of (a) the ice concentration (%) derived from visible images of sea-ice, and (b) sea/sea-ice surface temperatures (°C) derived from an infrared camera on 14 February.

indicated by an arrow in Figure 1 (lower panel). The ice cover decreased rapidly in the downwind region. In most images of the downwind region, there was no new ice or nilas, but there were many ripples and some low-level clouds (Figure 3c).

There were also many narrow open water areas on 18 February (Figure 5a). However, the concentration of ice is as a whole higher than that on 14 February and each open water area was distributed very sparsely. The low ice concentration in the most upwind region corresponds to the coastal polynya (upper panel in Figure 1). Although the aircraft was not able to reach the end of the marginal ice zone, i.e., open ocean on 18 February, Inoue et al. (2004) showed that the ice floe size became small from 10 to 2 m within the zone.

3.2. Sea-ice surface temperature

We also made surface radiation temperature measurements every 10 s (i.e., the horizontal resolution is approximately 1 km) by using an infrared camera. To reduce the error due to cloud contamination and absorption by water vapour as much as possible, we used the data measured at the lowest flight level.

Figure 4b shows the horizontal distribution of the surface temperature on 14 February. Within 60 km from the coast, the temperature was almost

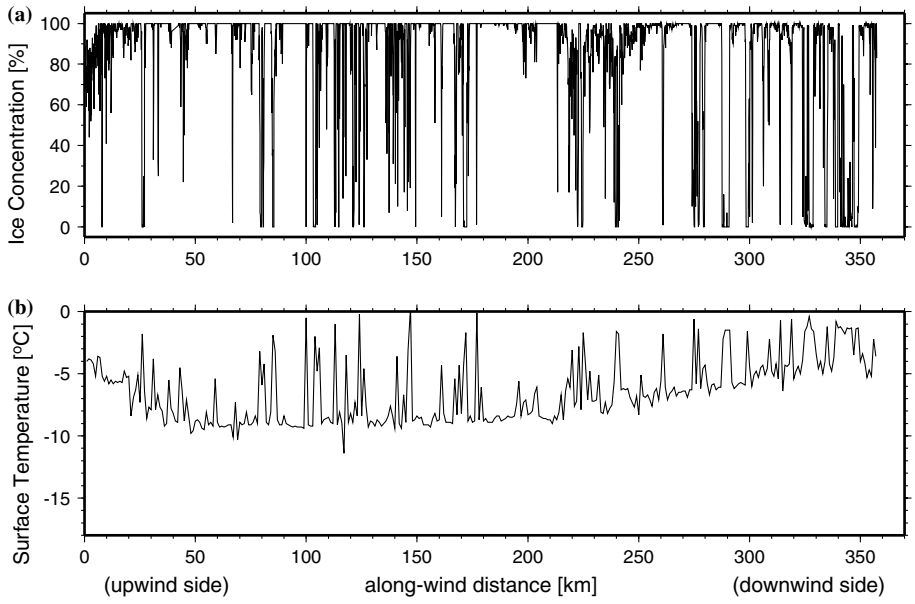

Figure 5. As for Figure 4, but on 18 February.

constant ($\approx -13\,^{\circ}$C) with some spikes of higher temperature. This suggests that the upwind region near the Sakhalin coast was generally covered with sea-ice. In contrast, in the middle part of the flight the temperature changed from -13 to $-3\,^{\circ}$C. The largest lead, of 10 km width (about 130 km offshore from the coast), can also be recognized as a high surface temperature area. The fluctuation of the temperature almost corresponds to that of the ice concentration (Figure 4a).

On 18 February (Figure 5b), the surface temperature also corresponded well with the ice concentration. In particular, there is a significant correlation between a high surface temperature and low ice concentration (i.e., leads). In the upwind region (within 50 km from the coast) the minimum surface temperature decreased from -4 to $-9\,^{\circ}$C. This result suggests that the ice thickness increases with increasing distance from the coastal polynya (upper panel in Figure 1).

4. Air-mass Modification

During vertical soundings of the atmosphere, high response measurements of the air temperature and absolute humidity were made continuously. Figure 6 shows the vertical profiles of air temperature and absolute humidity over the upwind and downwind regions on both days (the data below 400 m on 14

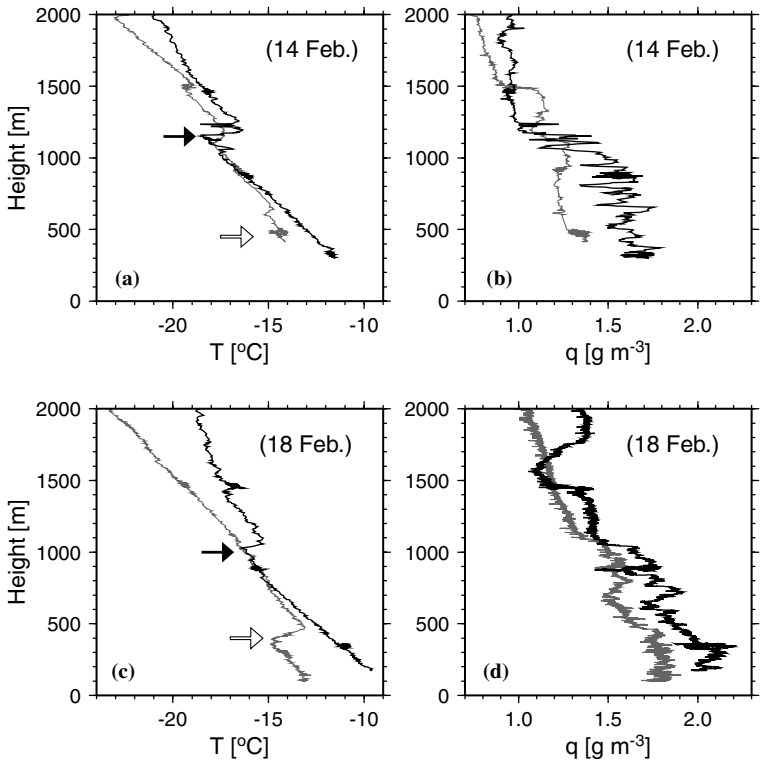

Figure 6. Vertical profiles of air temperature T and absolute humidity q on 14 and 18 February, 2000, respectively. Grey and black lines denote upwind and downwind vertical soundings, respectively. Each arrow denotes the level of an inversion layer.

February were missing due to mechanical troubles). The depth of the boundary layer increased from 450 to 1150 m on 14 February, and from 400 to 1000 m on 18 February. On 14 February, the moisture in the downwind region was well mixed below an inversion layer and decreased sharply above it. Such a mixing was not evident on 18 February, but the moisture showed a sharp decrease above the inversion layer. The increase of downwind air temperature and absolute humidity at the 400 m level by 2–3 K and 0.2–0.3 g m^{-3} indicates a supply of a large amount of sensible heat and moisture from the relatively warm sea surface below.

Figure 7 shows vertical cross-sections of air temperature constructed from the observations at three flight levels (200, 350 and 900 m), and relative humidity and ice concentration obtained by the lowest flight in both cases. The air temperature increased downwind at all levels, except for the 900-m level on 18 February. A rapid increase of air temperature occurred 90 km from the coast on 14 February. On the other hand, the air-mass modification gradually proceeded from the coast on 18 February. Differences between the

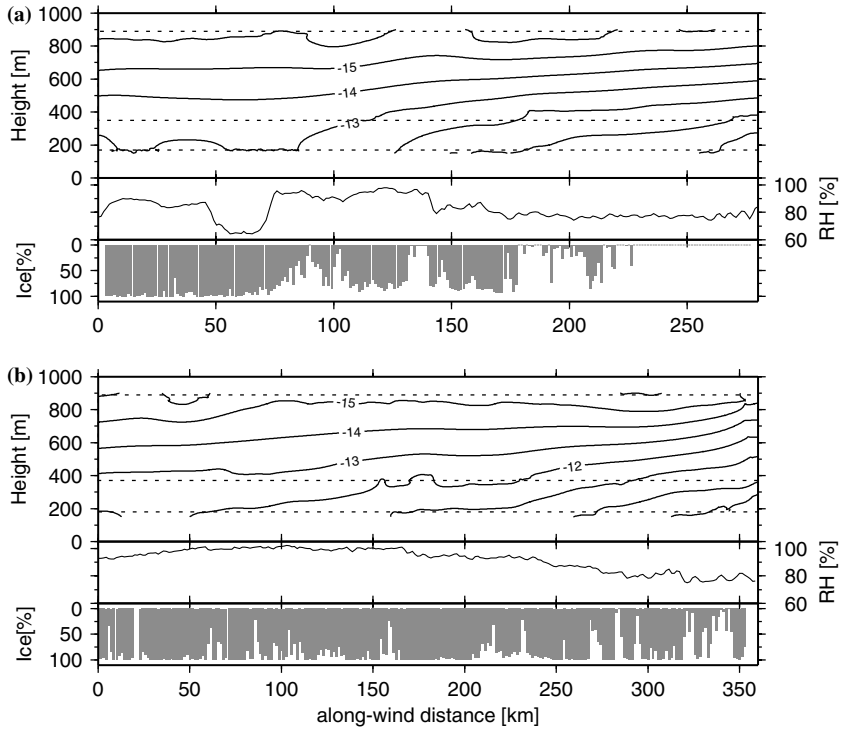

Figure 7. Vertical cross-sections of air temperature on (a) 14 February, and (b) 18 February. Each cross-section is drawn by interpolating the temperature on three level flights, shown by dotted lines. The lower two panels in both cases show the horizontal distribution of relative humidity at the lowest measuring level and the ice concentration.

two cases also existed in the distribution of relative humidity. The open water areas were concentrated around 90 and 130 km from the coast on 14 February, while they were sparsely distributed on 18 February.

As stated above, there were differences in air temperature, relative humidity and ice concentration between the two cases. However there was a common characteristic between them, involving the relationship between the air–sea temperature difference (ΔT) and the integrated extent of leads (L_o), i.e., the accumulated open water path. As mentioned before, the ice concentration rate (IC) was estimated every second and the aircraft speed was about 100 m s^{-1}. The accumulated open water path (L_o) is a function of the distance from the coast (x_R) and was calculated by integrating $(1 - IC)$ over the interval $[0, x_R]$ assuming that the horizontal scale of each point is 100 m in Figures 4a and 5a. ΔT was calculated assuming that the sea surface temperature was at the freezing point (−1.8 °C).

Figure 8 shows the change of ΔT with L_o on 14 and 18 February. There is an initial steep 2 K decrease of ΔT within 35 km, which corresponds to the

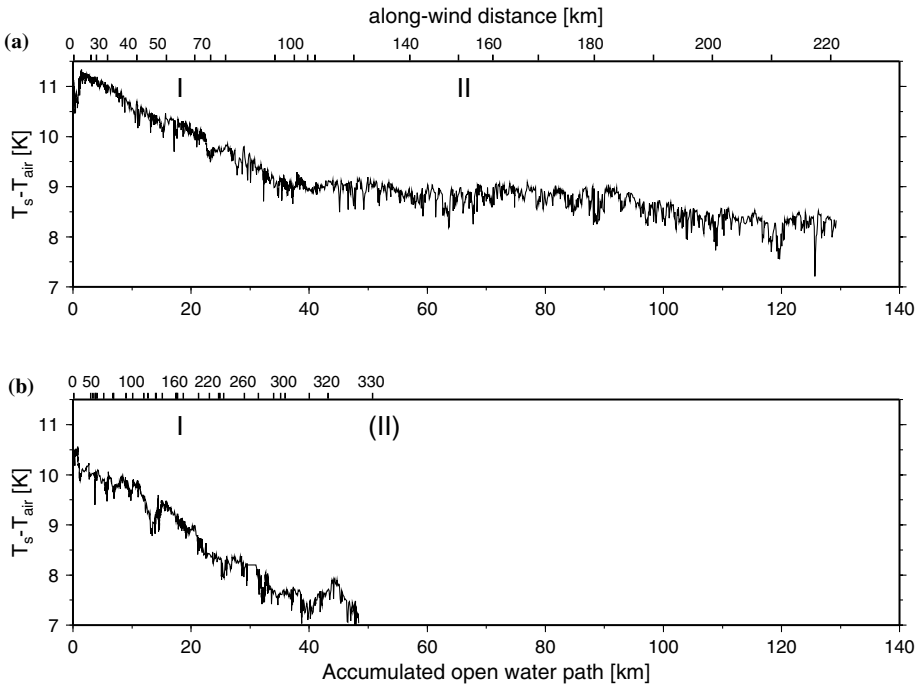

Figure 8. Temperature difference between sea-surface temperature (−1.8 °C) and air temperature (200 m level) as a function of accumulated open water path on (a) 14 February, and (b) 18 February. Upper abscissa represents the along-wind distance as shown in Figure 7.

area within 90 km from the coast on 14 February (Area I). Beyond the Area I, ΔT decreases very slowly with L_o (Area II). This suggests that active mixing occurred within the boundary layer in Area II. On 18 February, ΔT decreased with L_o up to 40 km in the same manner as on 14 February, but the region where ΔT decreased very slowly with L_o was almost unavailable due to the higher ice concentration. These results imply that numerous small leads also contribute to the air-mass modification and, therefore, high resolution measurement of sea-ice is indispensable for a quantitative estimation of heat flux from the sea surface.

5. Turbulent Heat Flux

Turbulent heat exchange between the sea surface and the overlying air is important, not only for the development of a boundary layer, but also for the cooling of the sea surface and resultant ice formation. In this section, we investigate the relationship between the heat flux and the accumulated fetch-width of open water (L_o) by using observations of the turbulent heat fluxes.

5.1. Measurement of turbulent heat fluxes

All measurements of the turbulence using the aircraft should be made on a horizontal flight path with a constant velocity and without any change of heading or roll. The gust probe on the aircraft provided the high-frequency turbulence, temperature and humidity fluctuations. The airborne pneumanemometer was used to measure true air speed, air temperature, and fluctuations along the horizontal flight direction component of wind speed based on a well-known gas dynamic equation (Dmitriev and Strunin, 1985). Dynamic pressure was measured by a device connected to a pitot pressure probe. Static pressure was measured by a pressure device connected to the static pressure holes of the aircraft. The aircraft clinometer was used to measure the fluctuations of the vertical component of the wind speed. Its operation was based on measurements of the fluctuation of attack angle, the pitch angle obtained by gyros, and the integration of the vertical aircraft acceleration (Strunin, 1997). The attack angle was measured with a spherical pressure device based on a relationship between the pressure difference in the holes on the sphere located in the airflow and the angle of the airflow distortion (Pahomov, 1962). Air humidity was measured by using ultraviolet and condensation hygrometers (Mezrin, 1997). The accuracy of these measurements is summarized by Strunin (1997).

When deviations of roll angle were more than 5° or changes of the aircraft velocity were more than 20 km h^{-1}, the data were omitted from the analysis. All turbulent fluctuations were measured over the frequency range from 0.06 to 8 Hz. This frequency range corresponded to the scale range from 12.5 to 1.7 km under the typical aircraft speed (100 m s^{-1}). All raw turbulence parameters (static pressure, dynamic pressure, differential pressure, air temperature, air humidity, and acceleration of the aircraft and pitch angle) were recorded with a frequency of 20 Hz. In the calculation of turbulent components, the mean value, and linear and parabolic trends were removed from the series of wind speed, air temperature and air humidity.

5.2. Method of analysis – joint frequency distribution technique

Since the buoyancy flux from the sea surface provides the primary energy source for the turbulent kinetic energy (e.g., Chou et al., 1986), quantitative estimation of its value in the lower boundary layer is important. The technique of joint frequency distribution has been used to study the buoyancy flux over warm oceans, for example, in the Air-Mass Transformation Experiment (AMTEX) by Mahrt and Paumier (1984) and the Genesis of Atlantic Lows Experiment (GALE) by Chou and Zimmerman (1989). Figure 9 shows the

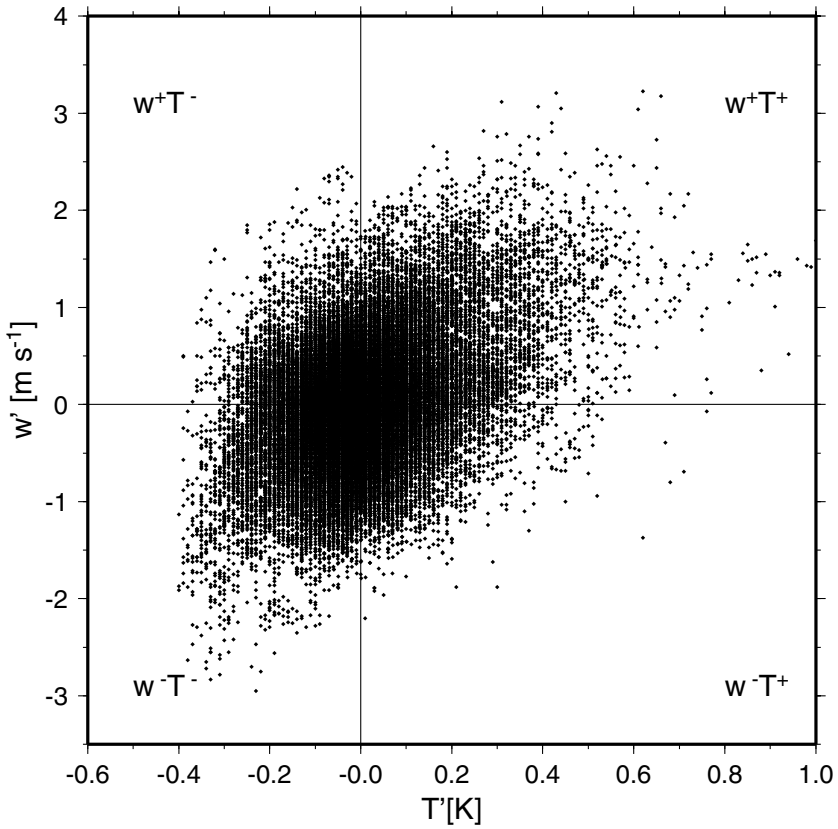

Figure 9. Scatter plots of T' and w' at the lowest flight level on 14 February. The number of sampling is 53,625.

scatter plots of w' and T' at the lowest flight level on 14 February. Here, the distribution of w' and T' is partitioned into four quadrants: warm updrafts (w^+T^+), cold updrafts (w^+T^-), warm down drafts (w^-T^+), and cold downdrafts (w^-T^-). As Chou and Zimmerman (1989) pointed out, the main physical processes contributing to these quadrants can be summarized as in Table I. The total buoyancy flux can be written as

TABLE I
Interpretation of physical processes of four quadrants in the joint frequency distribution.

Quadrant	Symbol	Process
Warm updraft	$\overline{w^+T_v^+}$	Thermal
Cold updraft	$\overline{w^+T_v^-}$	Penetrative convection
Warm downdraft	$\overline{w^-T_v^+}$	Compensating motion
Cold downdraft	$\overline{w^-T_v^-}$	Diabatic effect

$$\overline{w'T'_v} = \sum_{j=1}^{4} \frac{1}{N} \sum_{i=1}^{N_j} (w'T'_v)_i = \sum_{j=1}^{4} (\overline{w'T'_v})_j, \tag{1}$$

where N is the total number of observations of the time series, N_j the number of observations in the jth quadrant, and $(\overline{w'T_v'})_j$ the contribution to $\overline{w'T_v'}$. Each quadrant can be approximated by using the following equation (Stull, 1988),

$$\overline{w'T'_v} \simeq \overline{w'T'}(1 + 0.61\overline{q}) + 0.61\overline{T}\overline{w'q'}. \tag{2}$$

This method was applied to the observations at the lowest flight level in both cases. The heat flux was calculated from 100-s segments of the time series (i.e., $N = 2000$), which correspond to a 10-km length of the flight path (100 m s^{-1} $\times$ 100 s). The horizontal change of each component was obtained every 5 m (20 Hz) by shifting this 100-s segment.

Since we focus on the lead-induced sensible heat flux, the positive components ($\overline{w^+T_v^+}$ and $\overline{w^-T_v^-}$) are investigated in detail. A major advantage of the conditional sampling by separating $\overline{w^+T_v^+}$ and $\overline{w^-T_v^-}$ is that the major physical processes of heat transport can be understood by examining the ratio between $\overline{w^+T_v^+}$ and $\overline{w^-T_v^-}$. Further, the lead-induced sensible heat flux can also be estimated by using the ice concentration and $\overline{w^+T_v^+}$.

5.3. Horizontal change of turbulent heat fluxes

Figure 10a shows the horizontal distribution of $\overline{w'T'_v}$, $\overline{w^+T_v^+}$ and $\overline{w^-T_v^-}$ on 14 February. The contribution of $\overline{w^-T_v^+}$ and $\overline{w^+T_v^-}$ (not shown) are large in the area between 10 and 50 km from the coast and the total heat flux shows negative value (i.e., downward) there. However, the total heat flux becomes large (more than 50 W m^{-2}) in the lower ice concentration areas (between 80 and 110 km and between 130 and 150 km off the coast). In the downwind region over open water, about 100 W m^{-2} of the sensible heat flux was transported to the upper layer. As regards 18 February, on the other hand (Figure 10c), the values of $\overline{w'T'_v}$ and $\overline{w^+T_v^+}$ are smaller than those for 14 February due to the higher ice concentration (more than 40%).

Since the rising thermals are advected downwind by the ambient horizontal wind U, peaks of $\overline{w^+T_v^+}$ appeared slightly on the downwind side of the low ice concentration areas. The correlation coefficient between $\overline{w^+T_v^+}$ and ice concentration is -0.92 with a lag-distance ΔD = 3.6 km on 14 February, and -0.59 with ΔD = 7.6 km on 18 February, respectively. The mean ascending speed of thermals (w) from the surface to the 200 m level can then be estimated roughly by $w = U\Delta H/\Delta D$, where ΔH is the flight level (200m) and U is the horizontal wind speed ($U = 8.9$ and 10.9 m s^{-1} on 14 and 18 February, respectively). The estimated w on 14 February (0.49 m s^{-1}) is larger than that estimated for 18 February (0.29 m s^{-1}).

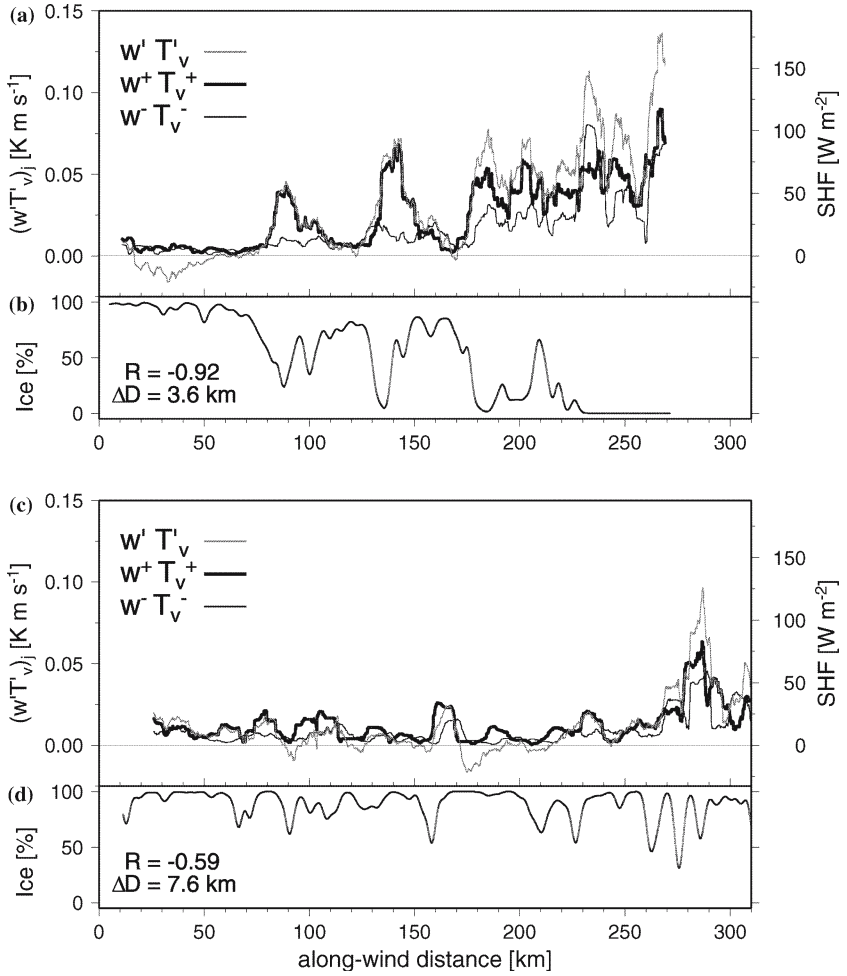

Figure 10. Horizontal distributions of $\overline{w'T'_v}$, $\overline{w^+T_v^+}$ and $\overline{w^-T_v^-}$, and 10 km of running mean ice concentration on 14 February (a and b), and 18 February (c and d). The ordinate on the right hand side represents the corresponding sensible heat flux (SHF). A letter R denotes the maximum correlation coefficient between ice concentration and $\overline{w^+T_v^+}$ with a lag-distance ΔD.

Contributions of $\overline{w^+T_v^+}$ and $\overline{w^-T_v^-}$ to $\overline{w'T'_v}$ are different between the upwind and downwind regions over the lower ice concentration area. Up to about 150 km from the coast on 14 February and 250 km from the coast on 18 February, $\overline{w^+T_v^+}$ was generally two or three times larger than that of $\overline{w^-T_v^-}$. On the other hand, in the downwind area, the ratio between $\overline{w^+T_v^+}$ and $\overline{w^-T_v^-}$ generally decreases downstream (except for 275 km offshore from the coast on 18 February), reflecting that the role of $\overline{w^-T_v^-}$ also becomes important. A larger contribution of $\overline{w^-T_v^-}$ to $\overline{w'T'_v}$ than that in the upwind

region implies the existence of strong downward motions of cold air associated with the development of the mixed layer.

Such a feature was also reported in the convective situation over a warm ocean [e.g., AMTEX (Mahrt and Paumier, 1984) and GALE (Chou and Zimmerman, 1989)]. The dominance of $\overline{w^+ T_v^+}$ in the total heat flux suggests that the mixing within the boundary layer is very weak and thermals are mainly responsible for the heat transport. Consequently, the air–sea temperature difference (ΔT) in the upwind open water decreases very quickly as shown in Figure 8 (Area I). On the other hand, ΔT decreases gradually in the downwind open water, because the mixing associated with the development of the boundary layer enhances $\overline{w^- T_v^-}$ (Area II in Figure 8).

Using the same method, the moisture flux ($\overline{w'q'}$) was also evaluated (figure 11). The correlation between the latent heat flux and ice concentration is relatively low compared with that of sensible heat flux (Figure 10). Further, little difference is noticeable in the contributions of $\overline{w^+ q^+}$ and $\overline{w^- q^-}$ to $\overline{w'q'}$ between the upwind and downwind areas. The amount of the latent heat flux is smaller than that of the sensible heat flux in both cases. The Bowen ratio, defined as $B = SHF/LHF$, varied from about 2 to 5. These high values of B were also reported in other marginal ice zones (e.g., Brümmer, 1996; Renfrew and Moore, 1999).

6. Concluding Remarks

Using two sets of aircraft observations during cold-air outbreaks, we studied the relationship between the extent of open water and air-mass modifications over the partially ice-covered Sea of Okhotsk. The turbulent heat flux over the ice-covered Sea of Okhotsk is discussed in conjunction with the accumulated fetch width, that is, the integral of each width of a lead.

The air–sea temperature difference (ΔT) dropped rapidly with the increase of the accumulated fetch-width of leads (L_o) up to about 35–40 km, then ΔT decreased very slowly with L_o. In spite of the difference in the horizontal distribution of ice concentration between the cases, this characteristic length is common, suggesting that the similar process for the onset of convective boundary layers exists under cold-air outbreak situations.

Using the joint frequency distribution method, the contributions of the rising thermals ($\overline{w^+ T_v^+}$) and cold downdrafts ($\overline{w^- T_v^-}$) to the total heat flux ($\overline{w'T'_v}$) were evaluated. A good correlation between the ice concentration and $\overline{w^+ T_v^+}$ was found in both cases. However, the ratio between $\overline{w^+ T_v^+}$ and $\overline{w^- T_v^-}$ differed significantly between upwind and downwind regions. In the upwind region with high ice concentration, the buoyancy flux was dominated by $\overline{w^+ T_v^+}$, while in the downwind region near the marginal ice zone $\overline{w^- T_v^-}$ also became important due to the development of the boundary layer. Considering

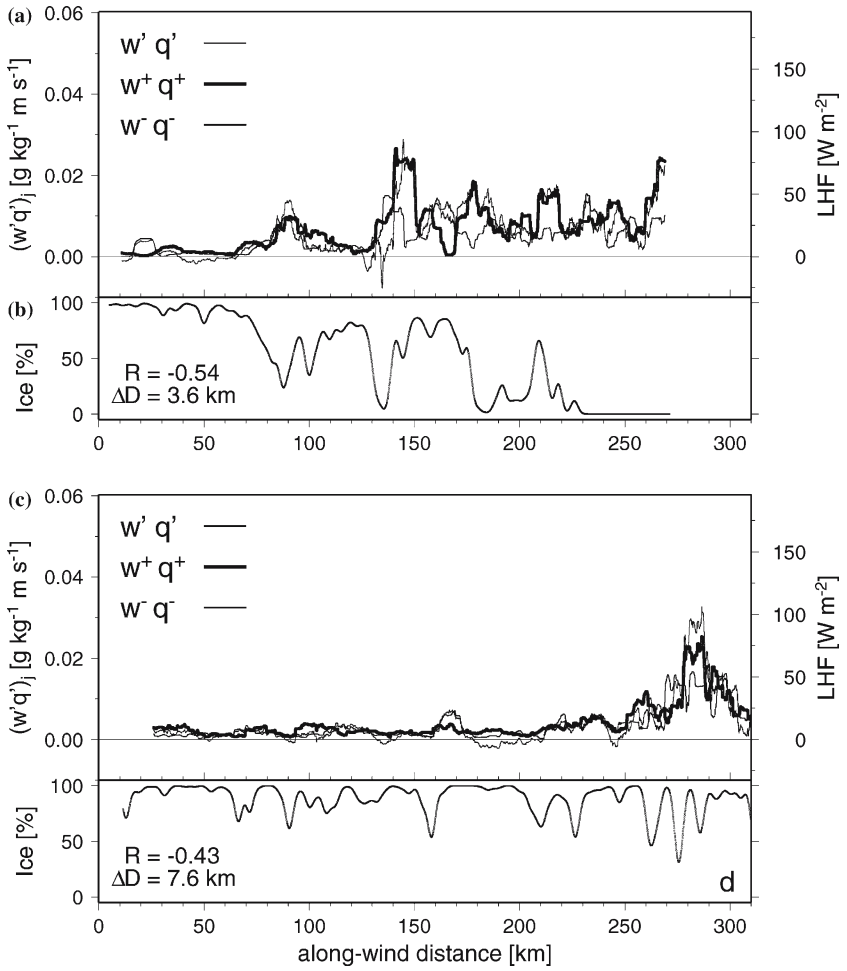

Figure 11. As for Figure 10, but for $\overline{w'q'}$. The ordinate on the right-hand side represents the corresponding latent heat flux (LHF).

the high Bowen ratio and relatively low correlation between the moisture flux ($\overline{w'q'}$) and ice concentration, the sensible heat flux had the most significant role for the air-mass modification over each lead.

Using the buoyancy flux ($\overline{w^+T_v^+}$) estimated in Section 5.3, the relationship between the total extent of open water and the sensible heat flux can be also examined. The sum of the heat flux from the sea and the ice surfaces, is expressed as follows:

$$\overline{w^+T_v^+} = \mathrm{IC}(\overline{w^+T_v^+})_\mathrm{i} + (1 - \mathrm{IC})(\overline{w^+T_v^+})_\mathrm{o} \tag{3}$$

where IC is the ice concentration ($0 \leq \mathrm{IC} \leq 1$), and $(\overline{w^+T_v^+})_\mathrm{i}$ and $(\overline{w^+T_v^+})_\mathrm{o}$ are the buoyancy flux originated from the ice surface and open water,

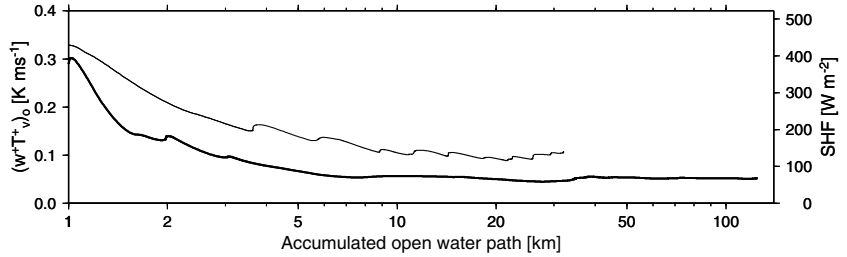

Figure 12. Horizontal average of $(\overline{w^+T_v^+})_o$ taken from the upwind region on 14 February (thick line), and 18 February (thin line). The ordinate on the right-hand side represents the corresponding sensible heat flux (SHF).

respectively. Assuming that the value of $(\overline{w^+T_v^+})_i$ is much smaller than that of $(\overline{w^+T_v^+})_o$ (e.g., Inoue et al., 2003), we can estimate the heat flux over leads by $(\overline{w^+T_v^+})_o \simeq \overline{w^+T_v^+}/(1 - \mathrm{IC})$. Figure 12 shows the buoyancy flux over leads $(\overline{w^+T_v^+})_o$ as a function of the accumulated fetch width. In both cases, the heat fluxes decrease from 400 to 100 W m^{-2} with increasing fetch width. The difference in their e-folding scale (about 3 and 9 km) between 14 and 18 February seems to come from the difference in both ice conditions and wind speed. However, the rapid decrease of the lead-integrated heat flux in both cases can be regarded as a typical situation in the ice-covered Sea of Okhotsk during cold-air outbreaks.

Although a coastal polynya has an important role in the formation of new ice, it can be regarded as a special case of the integral effect of leads. If the accumulated width of leads equals the width of a polynya, the integrated heat supply from narrow leads equals that from a coastal polynya. Therefore, high-resolution (about 10 m) measurement of leads is indispensable for a quantitative estimation of heat flux from the sea surface, and thus for an estimation of the formation of new ice. Based on our observational results, it is also inferred that the main region where new ice is actively formed would change from the early to later stages of a cold-air outbreak phase. New ice would be mainly formed within the partly ice-covered region in the early stage because of many leads within the region. On the contrary, in the later stage when almost all leads are covered with ice, new ice would be mainly formed in the marginal ice zone.

The results of this study are useful for the improvement of the processes of air–sea heat exchange included in air–ice–sea coupled models, and have significance for improving our understanding of the air–ice–sea interaction, not only on a local scale but also on a global scale.

Acknowledgements

We deeply appreciate the wonderful support given by A. Chernikov and M. Strunin at the Central Aerological Observatory of Russia while making

the aircraft IL-18 observations. The captain, officers and crew of the IL-18 are acknowledged for their good-natured support. We also thank K. Yamazaki, H. Enomoto, and K. I. Ohshima for their helpful suggestions. This study was supported by Core Research for Evolutional Science and Technology (CREST) from Japan Science and Technology Agency (JST), and a Research Fellowship of the Japan Society for the Promotion of Science for Young Scientists. A part of this work is based on a Ph.D. dissertation of J. I. at Hokkaido University, Japan.

References

Brümmer, B., Rump, B., and Kruspe, G.: 1992, 'A Cold Air Outbreak near Spitsbergen in Springtime – Boundary-Layer Modification and Cloud Development', *Boundary-Layer Meteorol.* **61**, 13–46.

Brümmer, B.: 1996, 'Boundary-Layer Modification in Wintertime Cold-air Outbreaks from the Arctic Sea Ice', *Boundary-Layer Meteorol.* **80**, 109–125.

Cavalieri, D. J. and Parkinson, C. L.: 1987, 'On the Relationship Between Atmospheric Circulation and the Fluctuations in the Sea Ice Extents of the Bering and Okhotsk Seas', *J. Geophys. Res.* **92**, 7141–7162.

Chou, S.-H., Atlas, D., and Yeh, E.-N.: 1986, 'Turbulence in a Convective Marine Atmospheric Boundary Layer', *J. Atmos. Sci.* **43**, 547–564.

Chou, S.-H. and Zimmerman, J.: 1989, 'Bivariate Conditional Sampling of Buoyancy Flux During an Intense Cold-air Outbreak', *Boundary-Layer Meteorol.* **46**, 93–112.

Curry, J. A., Schramm, J. L., and Ebert, E. E.: 1995, 'Sea Ice-Albedo Climate Feedback Mechanism', *J. Climate* **8**, 240–247.

Dmitriev, V. K. and Strunin, M. A.: 1985, 'The System of Introduction of Interdependent Corrections for Airplane Measurements of Wind Speed and Temperature of Air Fluxes', *Trudy TsAO* **158**, 104–112 (in Russian).

Honda, M., Yamazaki, K., Nakamura, H., and Takeuchi, K.: 1999, 'Dynamic and Thermodynamic Characteristics of Atmospheric Response to Anomalous Sea–ice Extent in the Sea of Okhotsk', *J. Climate* **12**, 3347–3358.

Inoue, J., Honda, M., and Kawashima, M.: 2001, 'Air Mass Transformation Processes over the Southwestern Region of the Ice-Covered Sea of Okhotsk during Cold Air Outbreaks', *J. Meteorol. Soc. Japan* **79**, 657–670.

Inoue, J., Ono, J., Tachibana, Y., Honda, M., Iwamoto, K., Fujiyoshi, Y., and Takeuchi, K.: 2003, 'Characteristics of Heat Transfer over the Ice-Covered Sea of Okhotsk During Cold Air Outbreaks', *J. Meteorol. Soc. Japan* **81**, 1057–1067.

Inoue, J., Wakatsuchi, M., and Fujiyoshi, Y.: 2004, 'Ice Floe Distribution in the Sea of Okhotsk in the Period when Sea-Ice Extent is Advancing', *Geophys. Res. Lett.* **31**, L20303, doi:10.1029/2004GL020809.

Iwamoto, K., Domon, K., Honda, M., Tachibana, Y., and Takeuchi, K.: 2001, 'Estimation of Surface Heat Flux Based on Rawinsonde Observation in the Southern Part of the Sea of Okhotsk Under Ice-Covered Condition', *J. Meteorol. Soc. Japan* **79**, 687–694.

Ledley, T. S.: 1988, 'A Coupled Energy Balance Climate Sea–ice Model: Impact of Sea Ice and Leads on Climate', *J. Geophys. Res.* **93**, 15919–15932.

Mahrt, L. and Paumier, J.: 1984, 'Heat Transport in the Atmospheric Boundary Layer', *J. Atmos. Sci.* **41**, 3061–3075.

Maykut, G. A.: 1978, 'Energy Exchange over Young Sea Ice in the Central Arctic', *J. Geophys. Res.* **83**, 3646–3658.

Mezrin, M. Y.: 1997, 'Humidity Measurements from Aircraft', *Atmos. Res.* **44**, 53–59.

Ohshima, K. I., Watanabe, T., and Nihashi, S.: 2003, 'Surface Heat Budget of the Sea of Okhotsk During 1987–2001 and the Role of Sea Ice on it', *J. Meteorol. Soc. Japan* **81**, 653–677.

Okubo, H. and Mannoji, N.: 1994, 'The Influence of the Sea Ice Distribution on the Surface Wind Forecast by Japan Spectral Model', *Tenki* **41**, 847–851 (in Japanese).

Pahomov, L. A.: 1962, 'Airplane Instrument for Measurement of Wind Speed', *Trudy TsAO* **41**, 62–71 (in Russian).

Renfrew, I. A. and Moore, G. W. K.: 1999, 'An Extreme Cold-Air Outbreak over the Labrador Sea: Roll Vortices and Air–sea Interaction', *Mon. Wea. Rev.* **127**, 2379–2394.

Smith, P. C. and MacPherson, J. I.: 1996, 'Airborne Surveys of the Atmospheric Boundary Layer Above the Marginal Ice Zone on the Newfoundland Shelf ', *Atmosphere–Ocean* **34**, 161–184.

Smith, S. D., Muench, R. D., and Pease, C. H.: 1990, 'Polynyas and Leads: An Overview of Physical Processes and Environment', *J. Geophys. Res.* **95**, 9461–9479.

Strunin, M. A.: 1997, 'Meteorological Potential for Contamination of Arctic Troposphere: Aircraft Measuring System for Atmospheric Turbulence and Methods for Calculation it Characteristics: Archive and Database of Atmospheric Turbulence', *Atmos. Res.* **44**, 17–35.

Stull, R. B.: 1988, *An Introduction to Boundary Layer Meteorology*, Kluwer Academic Publishers, Dordrecht.

Toyota, T., Kawamura, T., and Wakatsuchi, M.: 2000, 'Heat Budget in the Ice Cover of the Southern Okhotsk Sea Derived from In situ Observations', *J. Meteorol. Soc. Japan* **78**, 585–596.